CrossMark
click for updates

Modification of the carbide microstructure by N- and S-functionalization of the support in Mo$_x$C/CNT catalysts†

Benjamin Frank,‡ Zai-Lai Xie,§ Klaus Friedel Ortega,¶ Michael Scherzer, Robert Schlögl and Annette Trunschke*

A series of catalysts based on molybdenum carbide nanoparticles supported on carbon were prepared by carburization of an oxidic Mo precursor impregnated on differently treated multi-walled carbon nanotubes (CNTs) and reference carbons, respectively. The effects of surface defects and decoration of the support with heteroatoms (O, N, and S), as analyzed by IR and Raman spectroscopy as well as by TPD, were investigated. The catalysts were characterized by XRD, N$_2$ physisorption, and electron microscopy. The catalytic performance in steam reforming of methanol was used as a probe to indicate changes in the catalyst surface during catalytic action. The surface chemistry of the carbon supports influences the process of carburization and the nature of resulting supported Mo$_x$C (nano) particles. This includes crystal phase composition (α- and β-Mo$_x$C) and crystallite as well as particle diameter. However, if the surface decoration of the support is limited to oxygen groups, these differences are not reflected in the catalytic action, which is almost identical for oxygen functionalized carriers. A significant modification of the catalytic performance can only be achieved by surface modification of a CNT support with S- or N-containing functionalities, which causes changes in the lattice constant of the resulting carbide compared to reference systems. These changes are sensitively reflected in activity and CO$_2$/CH$_4$ product ratio in steam reforming of methanol.

Introduction

The catalytic performance of group VI metal carbides in hydrogen transfer reactions, such as hydrogenation, dehydrogenation, isomerization of alkanes, ammonia decomposition, Fischer–Tropsch synthesis, or electrocatalysis makes them highly attractive candidates for the substitution of expensive noble metals that are nowadays required for these processes.[1,2] The pure high surface area carbides for use in heterogeneous catalysis are accessible by controlled carburization of oxidic precursors,[3] whereas dispersed carbide

Department of Inorganic Chemistry, Fritz-Haber-Institut der Max-Planck-Gesellschaft, Faradayweg 4-6, D-14195 Berlin, Germany.
E-mail: trunschke@fhi-berlin.mpg.de; Tel: (+49)3084134457

† Electronic supplementary information (ESI) available: Analysis of catalytic performance data, full XRD patterns, SEM micrographs, and electron diffraction patterns. See DOI: 10.1039/c5cy01480h
‡ Current address: UniCat BASF Joint Lab (BasCat), Hardenbergstraße 36, 10623 Berlin, Germany.
§ Current address: State Key Laboratory of Photocatalysis on Energy and Environment, College of Chemistry, Fuzhou University, Fuzhou 35002, PR China.
¶ Current address: Faculty of Chemistry and CENIDE, Universität Duisburg-Essen, Universitätsstraße 5–7, 45141 Essen, Germany.

nanoparticles can also be stabilized on conventional high surface area support materials, such as carbon or alumina.[4–6]

The synthesis and application of carbon-supported molybdenum carbide catalysts has been frequently reported.[6–10] The dispersion of Mo$_x$C nanoparticles strongly depends on the carburization conditions such as heating rate and gas composition, but also on Mo loading and the degree of surface functionalization,[1b,6–8] which can be achieved, for example, by nitric acid treatment.[6] It is concluded that surface oxygen groups are needed to anchor the impregnated Mo precursor, although a systematic study has not been performed to investigate this effect in detail. A quantitative analysis indicates that the maximum loading of highly dispersed Mo species on the carbon surface is approximately 20 wt%,[8,11,12] which is supported by experimental data.[6,8]

Besides the structural stabilization of the carbide nanoparticles, the intrinsic structure and defect chemistry of the carbon support will also affect both the carburization process and product properties. From the reports of Solymosi *et al.* one can compare the catalytic activities of Mo$_2$C/C composites based on activated carbon[13] and on multi-walled CNTs,[5] respectively, in steam reforming of ethanol. An effect on both the activity and selectivity is observed showing that the CNT support lowers the activity but increases the selectivity to the

3468 | *Catal. Sci. Technol.*, 2016, **6**, 3468–3475

This journal is © The Royal Society of Chemistry 2016

target-product H_2. The characterization of the catalysts, however, is limited to X-ray photoelectron spectroscopy (XPS).

Our recent report[8] highlighted the impact of synthesis conditions, such as heating rate of the carburization in CH_4/H_2, composition of gas atmosphere, and Mo loading, on the physical and chemical properties and catalytic performance of CNT-supported Mo_xC catalysts in steam reforming of methanol (SRM). We showed that MoC/CNT is a stable catalyst under mild reaction conditions applied, whereas several previous studies pointed at the (partial) oxidation of the carbide phase in the presence of steam at higher temperatures and H_2O concentrations, respectively, or including metal dopants.[25a–d] Electronic and structural features of the CNT support might also play an important role here.[1b] In the present study, we focus on the impact of carbon surface properties, such as surface functionalization, in particular, incorporation of heteroatoms, defect density, and specific surface area on the nature of Mo_xC nanoparticles as well as their reactivity in steam reforming of methanol applied as probe reaction.

Experimental

Synthesis

Commercial multi-walled CNTs (Baytubes C 150 HP®) as well as reference multi-walled CNTs obtained from Shandong Dazhan were pre-treated by refluxing in 65% HNO_3 (500 ml per 10 g) for 2 h. The product was washed with deionized water until neutral pH and dried in air at 110 °C for 1 day (oCNT and oCNT(ref), respectively). 1 g of oCNT was further treated in a stream of 10% O_2/He at 673 K for 5 h[14] (O_2–oCNT) or stirred in 50 ml of 30% H_2O_2 at 65 °C for 24 h[15] (H_2O_2–oCNT), respectively. The pristine Baytubes were also treated in HNO_3 vapor (HNO_3–CNT).[16] Sidewall functionalization of Baytubes C150 HP® (Bayer) based on the diazotization of sulfanilic acid with isoamyl nitrite in water at 60 °C (molar ratio of CNT : sulfanilic acid = 1000 : 50) followed by removal of unreacted component through sonication and washing in 2,5-dimethylfuran resulted in S–oCNT. N-doped MWCNTs (Bayer)[17] were stirred in 3 M HNO_3 (100 ml per 1 g) at room temperature for 24 h, washed with deionized water until neutral pH and dried in air at 110 °C for 3 days (oNCNT). This mild acid treatment was also performed for high surface area nanographite (Timrex HSAG 300, oNG) and activated carbon (Chemviron Carbon 114A, oAC).

Aliquots of 1 g of each precursor were impregnated with 3 ml of a 117 mmol L^{-1} solutions of $(NH_4)_6Mo_7O_{24}\cdot 4H_2O$, respectively, to achieve a final Mo_xC loading of 20 wt%. Accordingly, samples are denoted as MoC/y-(o)CNT, where y identifies the treatment of the carbon support. The resulting pastes were thoroughly kneaded in a mortar followed by drying in air at 110 °C for 1 day.

In a typical carburization procedure, a catalyst mass nominally containing 0.5 mmol Mo (e.g., 250 mg MoC/oCNT) was placed in a quartz tubular reactor (7 mm inner diameter) in a stream of 37 ml min^{-1} of a 20 vol% CH_4/H_2 mixture. After elution of H_2O and O_2 the reactor temperature was linearly increased by 5 K min^{-1} up to 700 °C and kept for 2 h, followed by cooling to ambient temperature in the reducing atmosphere.

Characterization

Temperature-programmed desorption (TPD) of CO was performed immediately after carburization without passivation or air contact of the catalyst. The reactor was flushed with 5 vol% CO/Ar for 10 min at ambient temperature and subsequently flushed with He until no CO was detectable by on-line mass spectrometry (MS, Pfeiffer GAM 200) and gas chromatography (Varian CP-4900 Micro GC). In a He stream of 30 ml min^{-1} the temperature was linearly increased by 10 K min^{-1} up to 500 °C. Further characterization of the catalysts was performed after catalytic testing. Passivated samples were analysed by SEM and (HR)TEM, energy-dispersive analysis of X-rays (EDX), X-ray diffraction (XRD), and N_2 physisorption. SEM images were obtained with a Hitachi S-4800 FEG microscope (1.5 kV) equipped with an EDAX Genesis EDX detector (15 kV). TEM bright field images were taken with an Philips CM200 microscope equipped with an LaB6 cathode at an acceleration voltage of 200 kV. TEM data presented in ESI† were obtained with an image corrected Titan 80–300 Cs operated at 300 keV. For TEM analysis the samples were dry deposited onto holey carbon coated Cu grids. The XRD measurements were performed on a Bruker AXS D8 ADVANCE DAVINCI diffractometer equipped with a nickel filter and a LYNXEYE position sensitive detector (Cu $K\alpha_{1+2}$ radiation) in Bragg–Brentano geometry (fixed divergence slit). N_2 physisorption was performed at 77 K and p/p_0 = 0.05–0.3 after drying the sample in vacuum at 200 °C for 2 h. ATR-FTIR spectra were collected using a Varian 670 spectrometer fitted with a MCT detector and a germanium crystal (512 scans, 4 cm^{-1} resolution). The finely powdered specimen was deposited without diluent on the ATR crystal.

Catalytic testing

After CO TPD the catalysts were tested for their catalytic performance in the steam reforming of methanol (SRM) at 250 °C in 100 ml min^{-1} of a 1 vol% CH_3OH/1 vol% H_2O/He mixture. After 2 h on stream, the flow rate was varied between 100 and 10 ml min^{-1}, followed by decreasing the temperature in 10 K steps to 200 °C at 100 ml min^{-1}. Reaction products were quantified by GC analysis. Contact of the catalyst with H_2O (reactant) and CO_2 (product) ensured the mild passivation of the Mo_2C surface, which is required prior to final exposure of the catalyst to ambient for its characterization.

Results and discussion

Characterization of support materials

To investigate the impact of carbon surface properties on resulting Mo_xC/C catalysts a variety of support materials have been investigated. Based on the HNO_3-treated commercial

This journal is © The Royal Society of Chemistry 2016

Catal. Sci. Technol., 2016, 6, 3468–3475 | 3469

multi-walled CNTs (oCNT, Baytubes® C150HP)[8] different methods of surface treatment have been applied, which include oxidation processes as well as a specific decoration with sulfonic acid groups. Also the impact of N-doping of CNTs has been tested. Nano-graphite, activated carbon as well as a different type of CNTs serve as reference materials.

Nanostructured carbon supports used for Mo impregnation provide specific surface areas in the range of 200–350 $m^2 g^{-1}$ (Table 1) that justify a Mo_xC loading of 20 wt%.

The abundance of micropores in the activated carbon reference oAC results in a higher value of 741 $m^2 g^{-1}$. For nano-graphite (oNG), Raman spectroscopy (Fig. 1) reveals dominant features at around 1350, 1580, and 1620 cm^{-1}, referred to as D1, G, and D2 bands, respectively, indicating defective/amorphous (D1, D2) as well as crystalline/graphitic (G) carbon domains.[18] Notably, the rise of the G+ band in CNT-based materials at 1590 cm^{-1}, which is associated with C-atom vibrations along the c-axis of the tube[19] (see the corresponding range in IR spectra, Fig. 1), leads to a weak blue-shift of the superimposed G-feature. It is seen that oxidative post-treatment of oCNT further increases the specific surface area, which is accompanied by an increasing I_D/I_G ratio observed by Raman. The increase in surface area can thus be referred to surface roughness induced by oxidative etching of the CNT basal plane. Here, harsh vapor HNO_3 treatment (HNO_3–CNT) leads to substantial degradation documented by the highest I_D/I_G value of 2.75. oCNT(ref) shows higher crystallinity at a higher specific surface area (I_D/I_G = 1.98), pointing at a qualitative difference between both CNT precursor materials. On the other hand, acid-treated N-doped oN–CNTs are rich in bulk and surface structural defects, which is supported by TEM analysis showing a low degree of crystallinity and a significant fraction of fishbone carbon nanofibers.[17] The two reference materials nanographite oNG and activated carbon oAC were chosen due to very high and very low degree of structural order, respectively, with I_D/I_G ratios ranging from 1.67 to 15.01. The pronounced structural disorder in oAC and oN–CNT is supported by the appearance of a broad D4 band located at around 1200 cm^{-1} (Fig. 1).

The rich surface chemistry of functionalized carbon supports before Mo loading is documented in the content of O, N, and S atoms as determined by TPD (Table 1) as well as in infrared spectra (Fig. 1). It is supposed and intended that a significant fraction of N and S released during carburization (only up to 700 °C), is implemented in Mo_xC particles formed on these supports. Bands in the range of 1000–1320 cm^{-1} indicate C–O stretching vibrations attributed to alcohols, ethers, and carboxylic acids. These are dominating in oAC and absent in oNG, however, present in all other carbon supports. The high intensity of the corresponding bands in oAC is not due to a high surface density of the oxygen-containing functional groups, but related to the high specific surface area of oAC. A strong OH bending feature of carboxylic and sulfonic acid groups at 1423 cm^{-1} is visible for oCNT, oCNT(ref), and S–oCNT, whereas shoulders of this feature are weakly indicated in the spectra of the other materials.

The range of 1475–1600 cm^{-1} is dominated by aromatic C=C stretching vibrations of the graphitic lattice of the (nano)carbons. C=O stretching vibrations at 1670–1820 cm^{-1} are pronounced in the spectra of oCNT derived materials, oNG, and oAC. The oN–CNT material has no feature in this range, however, shows bands (shoulders) at 1279 and 1612 cm^{-1}, which can be interpreted as C_{aryl}–N stretching and N–H bending vibrations in amines, and C=N stretching vibrations, respectively. Instead, S–oCNT shows an additional broad band located at 1120 cm^{-1}, which is located in the typical range of asymmetric (1186 cm^{-1}) and symmetric (1062–41 cm^{-1}) S–O stretching vibrations of benzene sulfonic acid.[20] In Fig. 1 the frequency range up to 4000 cm^{-1} is not shown due to the absence of significant features according to C–H or O–H stretching vibrations.

Carburization of catalyst precursors

The catalyst precursors obtained by impregnation of the different supports with an aqueous solution of ammonium heptamolybdate (AHM) and subsequent drying have been carburized in a methane–hydrogen mixture. The processes of carburization of bulk and carbon supported Mo_xC catalysts in CH_4/H_2, H_2, and He atmospheres were discussed in detail in our previous studies.[8,21] Briefly, the following transformations can be identified from the H_2O traces recorded in the course of temperature-programmed carburization (Fig. 2): (i) decomposition of the AHM precursor into MoO_3, (ii) reduction of Mo^{VI} to Mo^{IV}, (iii) partial carburization of Mo^{IV} to a non-stoichiometric oxy carbide MoO_xC_y, and (iv) complete carburization of MoO_xC_y into Mo_xC. The profiles of H_2O evolution, the evolution of other gases (CO, CO_2) (not shown), as well as consumption of H_2 and CH_4 (not shown), i.e., peak positions and relative intensities, do not significantly differ for oxygen-functionalized carbon supports indicating that the process of carburization is similar on carbon materials doped with oxygen. Notably, the intensity of the final carburization peak (iv) correlates with the presence of poorly dispersed β-Mo_2C in the final catalysts as will be shown by XRD below.

A clear difference, however, is seen for the N-doped carbon support, where the carburization begins at lower

Table 1 Properties of carbon support materials[a]

Sample	S_{BET}/$m^2 g^{-1}$	I_D/I_G	O/mmol g^{-1}	S or N/mmol g^{-1}
oCNT	209	2.05	1.9	—
O_2–oCNT	323	2.48	1.4	—
H_2O_2–oCNT	270	2.47	1.9	—
HNO_3–CNT	342	2.75	2.9	—
oCNT(ref)	284	1.98	2.5	—
S–oCNT	226	2.27	1.1	0.39
oN–CNT	206	6.30	1.3	0.03 (6.8%[b])
oNG	303	1.67	1.6	—
oAC	741	15.01	3.5	—

[a] Heteroatom concentration determined from CO, CO_2, SO_2, NO, and N_2 release during TPD up to 850 °C. [b] $n_N/(n_N + n_C)$ as determined by EDX.

3470 | Catal. Sci. Technol., 2016, 6, 3468–3475
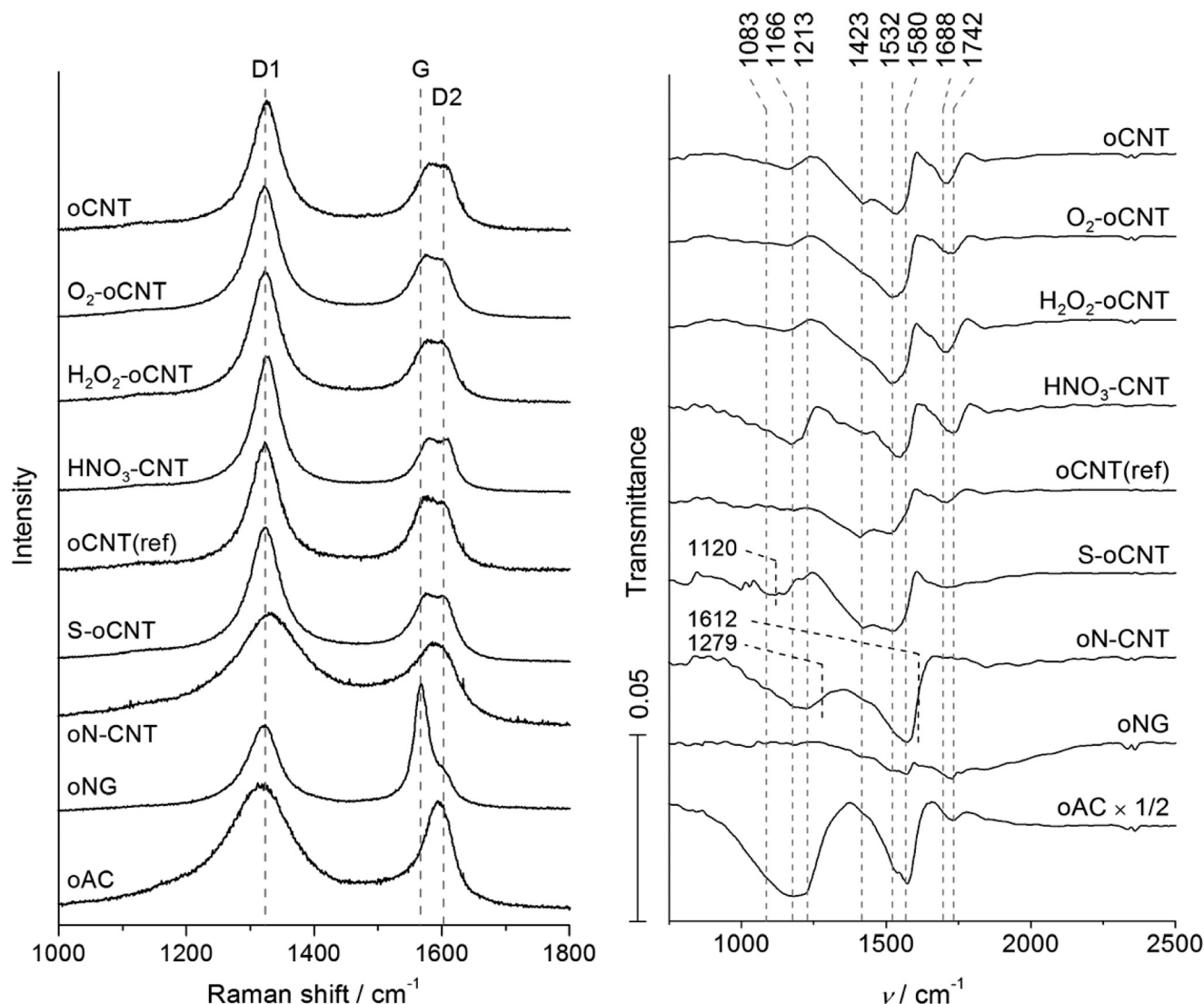
This journal is © The Royal Society of Chemistry 2016

Fig. 1 Normalized Raman spectra (left) and ATR spectra (right) of functionalized carbon support materials before impregnation with Mo precursor.
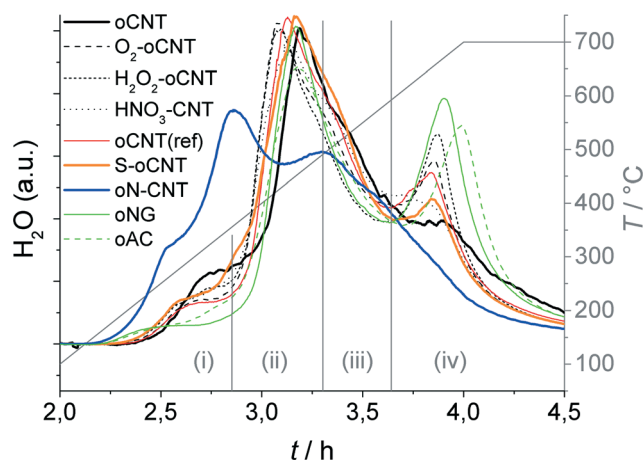

Fig. 2 Area-normalized MS traces of H_2O evolution (m/z 18) during carburization of carbon-supported Mo_xC catalysts.

temperature. The profile of H_2O evolution is broader and shows additional peaks. The incorporation of N into the Mo_xC lattice (nitridation) cannot be excluded. Features of initial AHM decomposition are seen on oN–CNT, whereas the final (bulk) carburization peak seems to exist only as a shoulder at the high-temperature edge of the main peak. The profiles suggest that N doping has a positive impact on the carburization as revealed by a peak shift to lower temperatures.

Reactivity in steam reforming of methanol

Steam reforming of methanol (SRM) was chosen as a probe reaction due to a complex selectivity pattern,[8] which is expected to sensitively indicate changes in the catalyst structure. In the reaction network of SRM, MeOH can react to CO_2 or CO,[22] which in the presence of H_2 can further react to CH_4 and higher alkanes/alkenes via Fischer–Tropsch synthesis over Mo-based catalysts.[23] At normal pressure, however, only small amounts of C_{2+} hydrocarbons (<5%) were detected.

This journal is © The Royal Society of Chemistry 2016

Catal. Sci. Technol., 2016, **6**, 3468–3475 | **3471**

Online-MS analysis of the reaction products reveals that the catalysts typically approach a stable catalytic performance after 2 h time-on-stream at 250 °C. The deactivation after 24 h is negligible. Fig. 3 (top) displays the MeOH conversion as a function of contact time. For MoC/oCNT the rapid increase in conversion is followed by a slow-down of the reaction rate after reaching ~50% conversion. This may be referred to inhibition by the main reaction products H_2 and CO_2 as observed over Cu-based catalysts.[24] Similar to previous reports[25,26] the reaction mainly yields CO_2, CO and CH_4. In the following, oxygen-functionalized carbons will be called heteroatom-free supports, since oxygen can be considered as a native surface modification. N-, and S-containing supports are referred to as heteroatom-doped materials. Surprisingly, all heteroatom-free carbon supported systems show almost identical activity in terms of MeOH conversion, which is a clear difference to a previous study comparing CNTs and activated carbon as support materials for Mo_xC catalysts.[25]
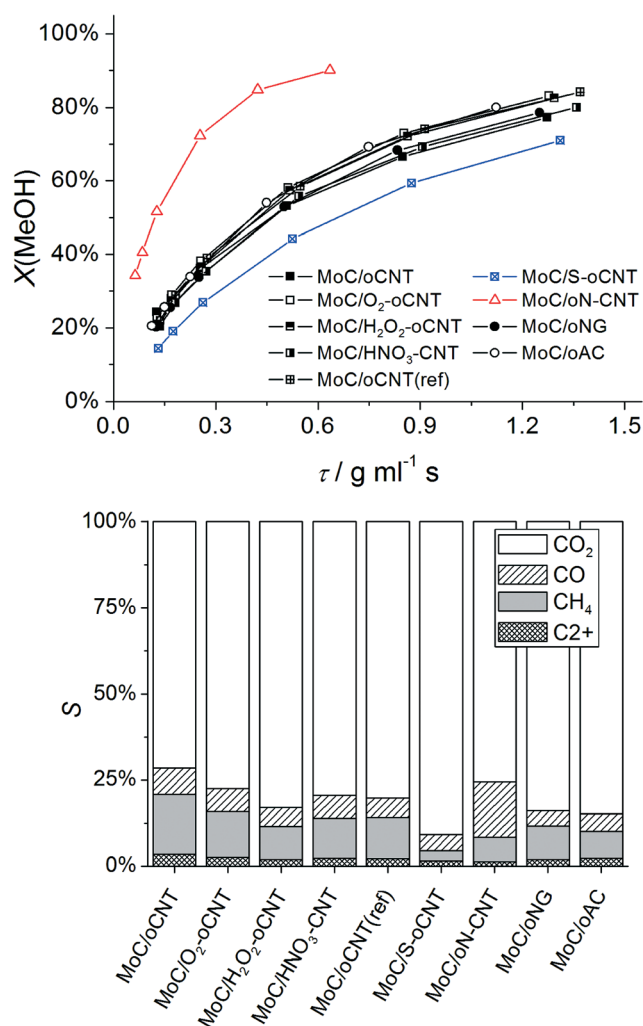
N-doping leads to higher activity, whereas S-doping reduces the activity.

The product selectivity at MeOH iso-conversion ($X = 50\%$) are shown in Fig. 3 (bottom). CO_2 is the main product, which is formed *via* steam reforming of methanol. CO and CH_4 are by-products formed *via* reverse water-gas shift and methanol decomposition or by methanol reduction and CO_x hydrogenation, respectively. Three parameters have been selected to quantify changes in the product selectivity of Mo_xC/C catalysts, namely the apparent activation energies of CO_2 and CH_4 formation, respectively, and the CO_2/CH_4 product ratio at $X(MeOH) = 50\%$ (Table 2). The CO_2/CH_4 ratio as a function of MeOH conversion (ESI,† Fig. S1) suggests that both CO_2 and CH_4 are primary products of the reaction; however, except for MoC/oN–CNT, secondary methanation of CO_2 also occurs. It is observed that all heteroatom-free carbon supported systems behave very similar. A significantly higher selectivity to CO_2 is obtained by using S–oCNT as the support, whereas the oN–CNT supported catalyst shows a CO_2/CH_4 ratio similar to heteroatom-free carbon supported systems, however, at a higher CO selectivity (Fig. 3 (bottom)). Fig. S1† furthermore reveals a different trend in product formation over MoC/oN-CNT, that is, increasing CO_2 selectivity with increasing MeOH conversion, which points at a different reaction network of parallel and consecutive reactions. Water-gas shift could play a dominant role here, transforming excess CO formed by MeOH decomposition into CO_2, whereas the methanation of CO and CO_2 appears less relevant. The apparent activation energies E_a determined for CO_2 and CH_4 formation explain the catalytic performance pattern. The CO_2/CH_4 product ratio strictly follows the difference $E_a(CH_4) - E_a(CO_2)$ (ESI,† Fig. S2). For heteroatom-doped S–oCNT and oN–CNT samples, the activities observed are in good agreement with observed Mo carbide dispersion as discussed later. N-doping of the carbon support increases both the Mo carbide dispersion and the resulting activity of the catalyst, whereas S-doping has the adverse effect. However, also electronic effects can contribute to the improved performance. For instance, it was found that small amounts of nitrogen (<5%) can strongly affect the rate of ammonia synthesis over both fcc and hcp Mo_xC catalysts.[27]

Fig. 3 Conversion of MeOH in the SRM reaction over carbon-supported Mo_xC catalysts as a function of the contact time; reaction conditions: 250 mg catalyst, 10–100 ml min^{-1} of 1% MeOH/1% H_2O/He, 250 °C (top); selectivity of the main reaction products at MeOH conversion of 50% (interpolated) (bottom).

Table 2 Catalytic performance of carbon-supported molybdenum carbide catalysts and textural properties of used samples

Sample[a]	E_a[b] (CO_2)	E_a[b] (CH_4)	$S(CO_2)/S(CH_4)$[c]	S_{BET}[d]	CO ads.[e]
MoC/oCNT	97	102	4.1	163	66.4
MoC/O$_2$–oCNT	93	104	5.8	173	79.5
MoC/H$_2$O$_2$–oCNT	91	106	8.6	137	20.8
MoC/HNO$_3$–CNT	93	107	6.9	136	47.0
MoC/oCNT (ref)	95	109	6.6	149	41.9
MoC/S–oCNT	85	109	30.9	145	6.5
MoC/oN–CNT	79	99	10.6	116	80.0
MoC/oNG	93	107	8.7	58	45.6
MoC/oAC	86	105	10.8	528	41.7

[a] Internal sample ID to clearly identify the catalyst batch are provided in ESI. [b] In kJ mol^{-1}. [c] $T = 250$ °C, $X(MeOH) = 50\%$. [d] In m^2 g^{-1}. [e] In μmol g^{-1}.

Accordingly, a bulk α-MoC$_{1-x}$ catalyst was reported to form a surface carbosulfide layer during hydrodesulfurization of thiophene, which lowers both CO adsorption capacity and catalytic activity.[28]

Post-catalytic characterization

After SRM tests the catalyst samples were characterized by XRD, N$_2$-physisorption, and electron microscopy. Due to the contact with H$_2$O and CO$_2$ acting as mildly oxidizing agents[29] during SRM no surface passivation by low-concentrated O$_2$ was needed prior to exposition to ambient conditions. XRD confirms the pervasive transformation of AHM into fcc α-MoC and hcp β-Mo$_2$C (Fig. 4). The full patterns are shown in the ESI† (Fig. S3). Nitride or sulfide phases are not observed, however, doping cannot be excluded. Although the catalysts have been used in a catalytic reaction involving potential oxidants such as H$_2$O or CO$_2$ and even after long-term exposition to ambient conditions the patterns give no rise to oxidic bulk phases. For comparison, the pattern of

molybdenum oxy carbide MoOC is characterized by a shift of the fcc pattern to higher angles,[30] which is indicative for a lattice contraction as a result of partial C–O-substitution. This is not the case here, where the detected peaks fall in line with the reference pattern for α-MoC.[31] Peak analysis reveals a crystallite diameter of approx. 1–2 nm.

The nature of the carbide phase strongly differs among the samples: oCNT, HNO$_3$–CNT, and oN–CNT supported carbide catalysts comprise mainly the cubic phase, whereas the reference supports oNG and oAC lead to the preferential formation of the hexagonal carbide structure. The oCNT derivatives O$_2$–oCNT, H$_2$O$_2$–oCNT, and S–oCNT, as well as oCNT(ref) result in a mixture of both phases, typically with an excess of fcc MoC. The reason for the formation of the metastable[32,33] α-MoC instead of β-Mo$_2$C, which is predominantly reported to form under the synthesis conditions applied,[3,4,6,29,34] is not fully understood. Han et al. suggest that the Mo$_x$C phase can be controlled over the Mo loading on an ordered mesoporous carbon (OMC) support.[9] However, presented XRD diffractograms are difficult to interpret. It is more likely that the controlled reduction of the Mo precursor is the key factor for α-MoC synthesis. This has been successfully managed by MoO$_3$ pre-reduction in a H$_2$/n-butane mixture,[33] or by adding 0.5% Pt to the Mo precursor to facilitate H$_2$ activation.[35] α-MoC proved a different performance than β-Mo$_2$C in some catalytic reactions[10,33,36] and is traditionally prepared via nitridation of MoO$_3$ with NH$_3$ to fcc γ-Mo$_2$N followed by subsequent re-carburization with CH$_4$.[35]

The specific surface areas of the CNT-based catalysts drop to 100–200 m^2 g^{-1}, which is caused by plugging of open CNT tips by agglomerates of MoC as well as by the much higher atomic mass of Mo as compared to C. The specific surface areas of MoC/oNG and MoC/oAC reference systems collapse to 58 and 528 m^2 g^{-1}, respectively. Having in mind similar activities and almost identical CO adsorption capacities for these samples (Table 2) we can exclude a significant impact of textural properties on the catalytic performances of MoC/C catalysts. For MoC/oCNT, the scanning (SEM) and transmission electron microscopy (TEM) analyses of the catalyst structure have been reported.[8] The finely structured agglomerates of very small (<5 nm) α-MoC crystallites are located preferably at the outer CNT surface and at their tips, which were previously opened by harsh HNO$_3$ treatment. They vary in size but rarely exceed a diameter of 10 nm. It was also shown that the CNT structure is intact after the carburization process,[8] which indicates that CH$_4$ rather than the support serves as the main carbon source for carbide formation. Similar results are obtained here: all nanotube-supported systems show the highly entangled structure without indication of significant MoC aggregation on the μm-scale, as exemplarily shown in the ESI† (Fig. S4a) for MoC/O$_2$–oCNT. Contrarily, the oNG and oAC supported catalysts show signs of agglomeration as indicated by high contrast areas in the SEM images (backscatter mode, see arrows in Fig. S4b and c†). The appearance of such tens of nanometers sized agglomerates correlates with pronounced high-temperature peaks of H$_2$O evolution during
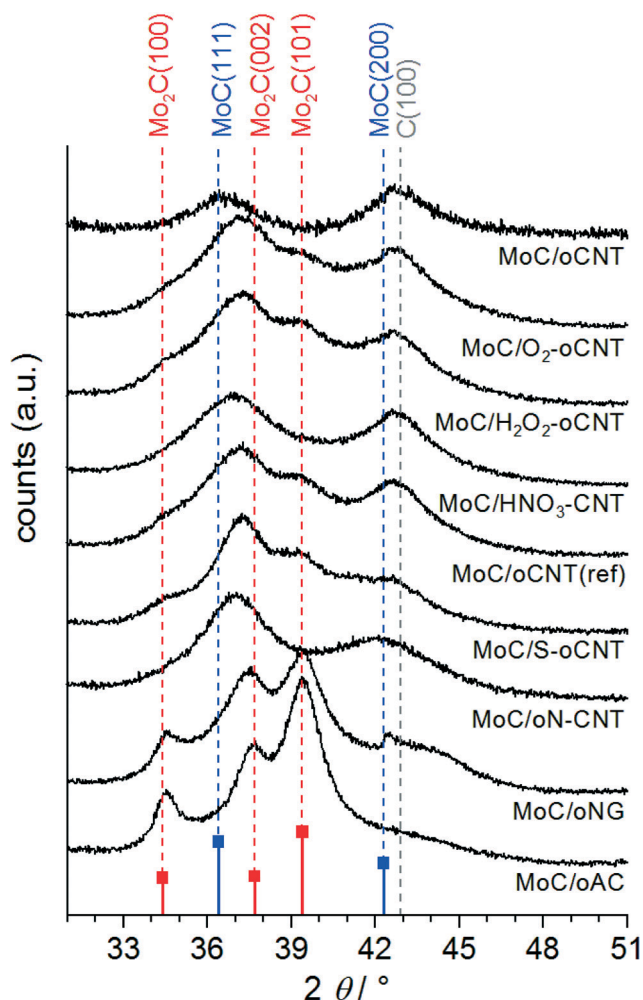

Fig. 4 XRD patterns of Mo$_x$C catalysts supported on differently functionalized carbon materials. Reference patterns: fcc α-MoC[33] (blue) and hcp β-Mo$_2$C (red).[37]

This journal is © The Royal Society of Chemistry 2016

Catal. Sci. Technol., 2016, 6, 3468–3475 | 3473

carburization (Fig. 2). Thus, we tentatively assign this feature to β-Mo$_2$C bulk carburization as the presence of large agglomerates also correlates with a significant fraction of β-Mo$_2$C (Fig. 4). Regarding the degree of surface functionalization (Table 1) an analogy exists between the interaction of the Mo precursor with the carbon surface and the nature of resulting supported MoC particles: well-anchored Mo species lead to finely dispersed nanoparticles of fcc α-MoC, whereas the poor interaction leads to large agglomerates of β-Mo$_2$C, however, without any consequences for SRM catalysis.

The only strong differences in catalytic performance have been observed when the supporting CNT's were doped either with nitrogen or sulfur. To understand the reason, a high-resolution TEM analysis has been performed. In agreement with CO adsorption (Table 2), molybdenum carbide particles are highly dispersed on the inner and outer surface of oN-CNT (Fig. 5). The particle size distribution is, however, quite broad comprising also larger particles (ESI,† Fig. S5). A similar high dispersion has been determined by CO adsorption on O$_2$–oCNT, while S–oCNT shows a particularly low dispersion (Table 2), which explains the lower activity of the latter catalyst.

Based on electron diffraction, lattice expansion and/or contraction has been identified in oN–CNT compared to the MoC/O$_2$–oCNT reference, which is less active in SRM in spite of similar dispersion according to CO adsorption (Table 2). The changes in lattice spacing might be an indicator for heteroatom doping of the carbide phase (see ESI,† Fig. S5 and Table S1). For the reference system MoC/O$_2$–oCNT the statistical error of d-spacing in supported Mo$_x$C nanoparticles is within ±1% and defines the accuracy of this method. Clearly, the N- and S-containing systems show significantly larger deviations of up to 5–10% if referred to the un-doped system. Of course, these depend on the crystal phase

considered (fcc or hcp), and it is far from a statistical analysis as only 5 particles per catalyst have been investigated. Nevertheless the results can be interpreted as a lattice distance modulation, which can be induced by heteroatom doping. This would be a reasonable explanation for the different catalytic behaviour observed in Fig. 3.

Conclusions

The preparation, characterization, and catalytic testing of CNT-supported Mo$_x$C catalysts are presented. The nature of the Mo$_x$C crystal phase is a sensitive function of the highly defective state of the carbon support structure, which kinetically controls the formation of favorable crystallization nuclei, leading to stabilized supported polycrystalline particles. The intimate interaction of the Mo precursor with the functionalized carbon surface leads to finely dispersed crystallites of α-MoC. For purely oxygen-decorated support materials, however, the nature of surface functionalization as well as the defect concentration or specific surface area is less relevant to the process of carburization. Instead, if the interaction is reduced by insufficient surface functionalization, larger agglomerates of β-Mo$_2$C are formed. All materials synthesized are highly active and stable catalysts in the steam reforming of methanol. However, the control over Mo$_x$C phase and particle and crystallite size, respectively, cannot be transferred to the catalytic performance in this specific reaction, although the catalyst is apparently stable under the action of H$_2$O and CO$_2$ in the reactive gas phase. A different picture is obtained as soon as heteroatoms such as N or S are introduced to the support. The carburization as well as catalytic performance is influenced to enable control over activity and CO$_2$/CH$_4$ selectivity. N-doping increases dispersion and activity, while S-doping functions in the opposite way. Some indication for heteroatom doping has been found in MoC/oN–CNT, which might be the key to enhanced activity of this catalyst compared to the likewise highly dispersed carbide particles in the reference material MoC/O$_2$–oCNT. However, further investigations are necessary to proof this hypothesis unambiguously.

Steam reforming of methanol was used as a probe reaction rather than as the economically/industrially interesting pathway for H$_2$ generation from liquid fuels. The experiments performed emphasise the impact of heteroatoms at the surface of nanostructured carbon supports on structure and catalytic performance of the supported phase. It is expected that trends and dependencies presented here to control the catalyst properties also provide important parameters to modify the activity and selectivity of CNT-supported Mo$_x$C catalysts in the synthesis of alcohols by hydrogenation of carbon monoxide.

Acknowledgements
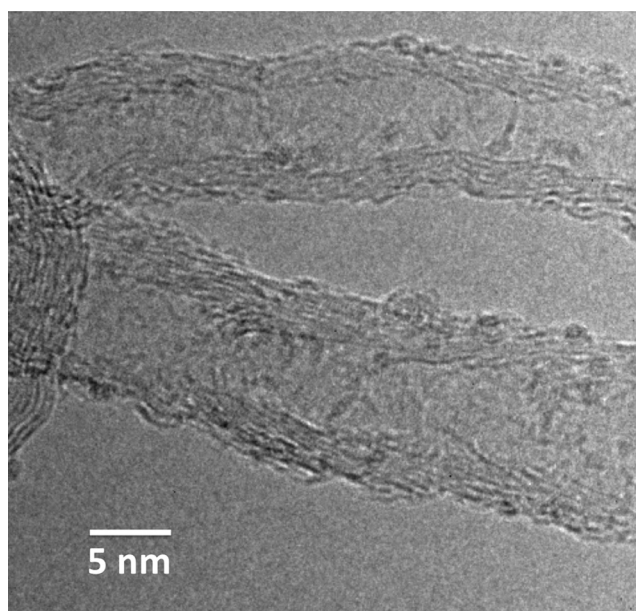
Fig. 5   HRTEM image of MoC/oN–CNT.

3474 | Catal. Sci. Technol., 2016, 6, 3468–3475

This journal is © The Royal Society of Chemistry 2016

References

1 (a) R. B. Levy and M. Boudart, *Science*, 1973, **181**, 547–549; (b) W.-F. Chen, C.-H. Wang, K. Sasaki, N. Marinkovic, W. Xu, J. T. Muckerman, Y. Zhu and R. R. Adzic, *Energy Environ. Sci.*, 2013, **6**, 943.

2 S. T. Oyama, in *Handbook of Heterogeneous Catalysis*, ed. G. Ertl, H. Knözinger, F. Schüth and J. Weitkamp, Wiley VCH, Weinheim, 2008, pp. 342–356.

3 J. S. Lee, S. T. Oyama and M. Boudart, *J. Catal.*, 1987, **106**, 125–133.

4 A. J. Brungs, A. P. E. York, J. B. Claridge, C. Márquez-Alvarez and M. L. H. Green, *Catal. Lett.*, 2000, **70**, 117–122.

5 R. Barthos, A. Széchenyi and F. Solymosi, *Catal. Lett.*, 2008, **120**, 161–165.

6 X. Li, D. Ma, L. Chen and X. Bao, *Catal. Lett.*, 2007, **116**, 63–69.

7 C. Sayag, M. Benkhaled, S. Suppan, J. Trawczynski and G. Djéga-Mariadassou, *Appl. Catal., A*, 2004, **275**, 15–24.

8 B. Frank, K. Friedel, F. Girgsdies, X. Huang, R. Schlögl and A. Trunschke, *ChemCatChem*, 2013, **5**, 2296–2305.

9 J. Han, J. Duan, P. Chen, H. Lou, X. Zheng and H. Hong, *ChemSusChem*, 2012, **5**, 727–733.

10 H. Wang, A. Wang, X. Wang and T. Zhang, *Chem. Commun.*, 2008, 2565–2567.

11 I. F. Silva, M. Klimkiewicz and S. Eser, *Energy Fuels*, 1998, **12**, 554–562.

12 Y.-C. Xie and Y.-Q. Tang, in *Advances in Catalysis*, Academic Press, 1990, pp. 1–43.

13 R. Barthos, A. Széchenyi, Á. Koós and F. Solymosi, *Appl. Catal., A*, 2007, **327**, 95–105.

14 B. Frank, A. Rinaldi, R. Blume, R. Schlögl and D. S. Su, *Chem. Mater.*, 2010, **22**, 4462–4470.

15 Y. Peng and H. Liu, *Ind. Eng. Chem. Res.*, 2006, **45**, 6483–6488.

16 W. Xia, C. Jin, S. Kundu and M. Muhler, *Carbon*, 2009, **47**, 919–922.

17 A. Wolf, V. Michele, L. Mleczko, J. Assmann and S. Buchholz, *Method for Producing Nitrogen-Doped Carbon Nanotubes*, Patent US20100276644, 2010.

18 A. Sadezky, H. Muckenhuber, H. Grothe, R. Niessner and U. Pöschl, *Carbon*, 2005, **43**, 1731–1742.

19 M. S. Dresselhaus, G. Dresselhaus, R. Saito and A. Jorio, *Phys. Rep.*, 2005, **409**, 47–99.

20 G. Świderski, M. Kalinowska, R. Świsłocka, S. Wojtulewski and W. Lewandowski, *Spectrochim. Acta, Part A*, 2013, **100**, 41–50.

21 T. Cotter, B. Frank, W. Zhang, R. Schlögl and A. Trunschke, *Chem. Mater.*, 2013, **25**, 3124–3136.

22 Á. Mastalir, Á. Patzkó, B. Frank, R. Schomäcker, T. Ressler and R. Schlögl, *Catal. Commun.*, 2007, **8**, 1684–1690.

23 M. Saito and R. B. Anderson, *J. Catal.*, 1980, **63**, 438–446.

24 B. Frank, F. C. Jentoft, H. Soerijanto, J. Kröhnert, R. Schlögl and R. Schomäcker, *J. Catal.*, 2007, **246**, 177–192.

25 (a) R. Barthos and F. Solymosi, *J. Catal.*, 2007, **249**, 289–299; (b) Y. Ma, G. Guan, X. Hao, Z. Zuo, W. Huang, P. Phanthong, K. Kusakabe and A. Abudula, *RSC Adv.*, 2014, **4**, 44175; (c) Y. Ma, G. Guan, P. Phanthong, X. Hao, W. Huang, A. Tsutsumi, K. Kusakabe and A. Abudula, *J. Phys. Chem. C*, 2014, **118**, 9485; (d) Y. Ma, G. Guan, C. Shi, A. Zhu, X. Hao, Z. Wang, K. Kusakabe and A. Abudula, *Int. J. Hydrogen Energy*, 2014, **39**, 258.

26 S. S.-Y. Lin, W. J. Thomson, T. J. Hagensen and S. Y. Ha, *Appl. Catal., A*, 2007, **318**, 121–127.

27 R. Kojima and K. Aika, *Appl. Catal., A*, 2001, **219**, 141–147.

28 J. S. Lee and M. Boudart, *Appl. Catal.*, 1985, **19**, 207–210.

29 W. Wu, Z. Wu, C. Liang, P. Ying, Z. Feng and C. Li, *Phys. Chem. Chem. Phys.*, 2004, **6**, 5603.

30 I. F. Ferguson, J. B. Ainscough, D. Morse and A. W. Miller, *Nature*, 1964, **202**, 1327–1328.

31 O. Matsumoto, Y. Yaguchi, Y. Shiota and Y. Kanzaki, *High Temp. Sci.*, 1983, **16**, 243–250.

32 H. O. Pierson, in *Handbook of Refractory Carbides & Nitrides*, Noyes Publications, New Jersey, 1997, pp. 110–112.

33 C. Bouchy, I. Schmidt, J. R. Anderson, C. J. H. Jacobsen, E. G. Derouane and S. B. J. Derouane-Abd Hamid, *J. Mol. Catal. A: Chem.*, 2000, **163**, 283–296.

34 A. Hanif, T. Xiao, A. P. E. York, J. Sloan and M. L. H. Green, *Chem. Mater.*, 2002, **14**, 1009–1015.

35 J. S. Lee, L. Volpe, F. H. Ribeiro and M. Boudart, *J. Catal.*, 1988, **112**, 44–53.

36 G. S. Ranhotra, A. T. Bell and J. A. Reimer, *J. Catal.*, 1987, **108**, 40–49.

37 B. Lönnberg, *J. Less-Common Met.*, 1986, **120**, 135–146.

This journal is © The Royal Society of Chemistry 2016

Catal. Sci. Technol., 2016, **6**, 3468–3475 | **3475**